



**HAL**  
open science

## Modelling of stylolite geometries and stress scaling

Daniel Koehn, Marcus Ebner, Francois Renard, Renaud Toussaint, C. W. Passchier

► **To cite this version:**

Daniel Koehn, Marcus Ebner, Francois Renard, Renaud Toussaint, C. W. Passchier. Modelling of stylolite geometries and stress scaling. *Earth and Planetary Science Letters*, 2012, 341-343, pp.104-113. 10.1016/j.epsl.2012.04.046 . hal-00701975

**HAL Id: hal-00701975**

**<https://hal.science/hal-00701975>**

Submitted on 28 May 2012

**HAL** is a multi-disciplinary open access archive for the deposit and dissemination of scientific research documents, whether they are published or not. The documents may come from teaching and research institutions in France or abroad, or from public or private research centers.

L'archive ouverte pluridisciplinaire **HAL**, est destinée au dépôt et à la diffusion de documents scientifiques de niveau recherche, publiés ou non, émanant des établissements d'enseignement et de recherche français ou étrangers, des laboratoires publics ou privés.



31 Keywords: stylolite, stress-gauge, compaction, pressure solution, numerical model, self-  
32 affinity

33

### 34 **1. Introduction**

35 Pressure solution is an important deformation mechanism that takes place in the upper parts  
36 of the Earth's crust (Rutter, 1983). This mechanism of dissolution, transport and precipitation  
37 of material starts as shallow as 90m during diagenesis in sedimentary basins (Tada & Siever  
38 1989) and may still be active during high grade metamorphic conditions (Beach, 1979). If the  
39 dissolution of material takes place in a localized manner, rough dissolution surfaces develop  
40 that are termed stylolites (Fig. 1, Dunnington, 1954; Heald, 1955; Park & Schot, 1968;  
41 Guzzetta, 1984; Merino, 1992; Railsback, 1993; Karcz & Scholz, 2003). Stylolites are very  
42 common in a variety of mono-mineralic rock types and have several distinct characteristics:  
43 they concentrate material that cannot be dissolved as fast as the matrix appearing as dark  
44 seams, the surface has a pronounced roughness of peaks or spikes with parallel or inward  
45 sloping sides, such that they can be pulled apart without breaking the rock; and this roughness  
46 occurs on a range of scales (Fig. 1).

47 Geologists are interested in stylolites because they are used to estimate the compaction and  
48 the stress history in sedimentary basins (Ebner et al. 2009b, Petit & Mattauer 1995, Rispoli  
49 1981). The hydrocarbon industry is mainly interested in stylolites because they affect  
50 reservoir properties; they can be sealing because of their clay content and reduce porosity and  
51 permeability around the stylolite, while they may also act as channel-ways when fluids travel  
52 along the stylolite interface (Fabricius & Borre, 2007; Baron & Parnell, 2007). The use of  
53 stylolites to estimate compaction and stress is of great interest to Earth scientists and may be  
54 used for basin analysis or tectonic studies in fold and thrust belts. Reliable paleo-stress gauges  
55 are rare in geology. For several reasons we are convinced that stylolites can play this role: (1)  
56 Stylolites are very common geological structures and (2) the orientation of their teeth track

57 the direction of the main compressive stress, (3) the magnitude of these asperities capture part  
58 of the compaction history of the host-rock and (4) it has been demonstrated that the stylolite  
59 roughness can be used to estimate absolute stress values, i.e. the mean, differential and the  
60 principal stress values (Ebner et al., 2009b, 2010a). A few other paleo-stress markers exist, as  
61 e.g. the study of calcite twins in rocks (Burkhard. 1993, Lacombe, 2010), but they are  
62 generally more sensitive to the stress orientation than to its magnitude. It is useful to develop  
63 additional paleo-stress gauges, which can be applied on a variety of rocks, such as stylolites  
64 that are present in many sedimentary rocks.

65

## 66 **2. The use of stylolites for structural analysis**

67 Stylolite morphology develops according to two main processes. Firstly, an interface can  
68 either be initially present in the sediment, such as the interface between two different  
69 sedimentary layers or a fracture, or they form by propagation from an initial site of stress  
70 concentration that promotes the formation of an anticrack (Fletcher and Pollard, 1981),  
71 localize due to chemical effects induced by micas (Aharonov and Katsman 2009) or localized  
72 volume reduction (Katsman et al. 2006). Secondly, such interface may roughen with time, a  
73 process that is dependent on local stress conditions and the amount of heterogeneities in the  
74 rock. Stylolites can be used in structural analysis to find three parameters: the main  
75 compressive stress direction (e.g. Rispoli, 1981, Koehn et al. 2007), the amount of  
76 compaction and the product of the differential and mean stress (Ebner et al, 2009b, Ebner et  
77 al. 2010a). Stylolite teeth (Fig. 2a) are thought to grow parallel to the main compressive stress  
78 direction, a hypothesis that was strengthened by recent numerical simulations (Ebner et al.  
79 2009a, Koehn et al. 2007). These simulations show that the lateral position of a tooth along a  
80 stylolite interface is random but its shape is strongly deterministic with respect to the  
81 orientation of the direction of maximum finite compaction, which is identical with the main  
82 compressive stress orientation in homogeneous solids. The amplitude of a stylolite can be

83 used indirectly to calculate the amount of compaction. Although this can be difficult, the non-  
84 linear scaling relationship between finite compaction and average stylolite amplitude gives  
85 reasonable estimates (Koehn et al. 2007). Without the use of a scaling function one can  
86 estimate the amount of dissolved material at the stylolite by using its maximum height, but  
87 this requires the observation of this maximum in a few spots, which can be hidden in the rock  
88 in some situations. Hence, the maximum height observed corresponds to a lower bound of the  
89 dissolution (amount of compaction along the stylolite) that took place, and not necessarily the  
90 total one. The scaling function given by Koehn et al. (2007) can be used to estimate  
91 compaction; however the function is non-linear leading to a relatively large uncertainty in the  
92 result.

93 The third and most important value that can be determined from natural stylolites is the  
94 product of the differential and mean stress, which can be calculated from the scaling of the  
95 stylolite roughness (Renard et al., 2004), based on an analytical solution presented in  
96 Schmittbuhl et al. (2004). This analytical solution demonstrates that the stresses acting during  
97 stylolite formation can be derived from the stylolite roughness hidden in the crossover-length  
98 scale that separates two self-affine scaling regimes well documented for natural stylolites.  
99 Ebner et al. (2009b) showed in a study on natural bedding parallel stylolites, which were  
100 sampled at different depths in a sedimentary basin, that the measured principal normal stress  
101 value increases linearly with the depth of stylolite formation, which supports the analytical  
102 solution. These authors also present a method that allows the calculation of the full paleo-  
103 stress tensor from the stylolites under favourable conditions. In addition Ebner et al. (2010a)  
104 show with a study on tectonic stylolites that these can reveal the difference between all three  
105 principal stress components, which is an additional support for the theory of Schmittbuhl et  
106 al. (2004).

107 In order to further test the hypothetical scaling relation of the stylolite roughness as a function  
108 to overburden stress, we present two-dimensional numerical simulations of the roughness

109 development of a set of sedimentary stylolites and their sensitivity to stress. First we present  
110 different stylolite geometries that develop in a limestone with a constant grain size versus a  
111 limestone with a bimodal distribution of grains (or fossils). Then we test the analytical  
112 solution of Schmittbuhl et al. (2004) and show with a numerical model (Koehn et al., 2007)  
113 how stylolites can be used to attain the full paleo-stress tensor and the paleo-depth of  
114 (bedding parallel) stylolite growth in a sedimentary basin. In addition we validate our  
115 numerical simulations by showing that they result in stylolite geometries found in nature and  
116 we show that the model reproduces the crossover length scale that is predicted by the solution  
117 of Schmittbuhl et al. (2004) for a given stress.

118

### 119 **3. The stress gauge**

120 Detailed measurements of stylolite roughness (Renard et al. 2004, Ebner et al. 2009b), as well  
121 as deterministic models of stylolite formation (Schmittbuhl et al. 2004, Koehn et al. 2007)  
122 indicate that the absolute value of the stress can be determined from the roughness of a  
123 stylolite. Stylolites are thought to roughen because of the existence of heterogeneities in a  
124 rock that dissolve at different rates than the host-rock. In limestone, these heterogeneities may  
125 be fossils on a millimetre scale or clay particles, oxide or quartz grains on a micrometer scale.  
126 Impurities are localizing dissolution and in some cases enable stylolite formation (Aharonov  
127 and Katsman, 2009) and collect within the stylolite surface during successive stress driven  
128 dissolution of the host-rock. The host-rock dissolves on both sides of the stylolite. If this  
129 dissolution is locally heterogeneous, so that one part of the host-rock on one side of the  
130 stylolite dissolves slower than the other, the interface starts to become rough (Fig. 2a,b). In an  
131 extreme case an impurity like an oxide grain can pin one side of the stylolite host-rock  
132 completely, so that this side does not dissolve at all. The pinning particle is then quasi pushed  
133 into the host-rock on the other side of the stylolite and a spike develops. For example, Ebner

134 et al. (2010b) have shown with an EBSD analysis that small quartz grains pin corners of some  
135 stylolite teeth (Fig. 2c).

136 The developing stylolite roughness can be accurately described by a self-affine scaling  
137 function with a characteristic Hurst or roughness exponent (Brouste et al. 2007, Gratier et al.  
138 2005, Renard et al. 2004, Schmittbuhl et al. 2004). When a rough surface shows a self-affine  
139 property, its roughness has a variable amplitude ( $A$ ) over wavelength ( $\lambda$ ) ratio at different  
140 scales. A self-affine 1D profile can be described mathematically as invariant under self affine  
141 transformations, i.e. anisotropic zooms of any pair of factors  $(b, b^\alpha)$ , where  $b$  is real,  
142 respectively for the sub-parallel and normal direction to the average surface: A zoom  
143 transformation on the surface in the  $x$ -direction by  $x \rightarrow bx$  and in height by  $h \rightarrow b^\alpha h$ , where  $x$   
144 is oriented parallel to the stylolite interface,  $h$  is the height of the interface,  $b$  is a linear  
145 scaling factor and  $\alpha$  the Hurst or roughness exponent (Barabasi & Stanley 1995). If the  
146 roughness exponent is smaller than 1.0 the profile is called self-affine: it appears flat on the  
147 large scale and rougher (with larger aspect ratio  $A/\lambda$  of out of plane amplitude over in plane  
148 wavelength) on the small scale. Such a scaling is reproduced by the natural stylolite shown in  
149 Figure 1, where the stylolite seems flat on the larger scale (Fig. 1a, width 40cm, low ratio  
150  $A/\lambda$ ) and appears progressively rougher on the small scale (Fig. 1c,d, width 6cm and 4mm,  
151 higher ratio  $A/\lambda$ ). Natural stylolites tend to show not only one but two characteristic  
152 roughness exponents. On the large scale the exponent is around 0.5 whereas on the small  
153 scale it is close to 1 (Renard et al., 2004, Schmittbuhl et al. 2004). The change from one  
154 scaling regime to the other (characterized by different scaling exponents) is relatively sharp. It  
155 lies typically on the millimetre length scale and is termed crossover-length ( $l$ ). An interface  
156 with a roughness exponent of about 1.0 is called self-similar, and does not change its  
157 roughness aspect ratio  $A/\lambda$  with different scales, which can also be seen in Figure 1c,d, where  
158 the amplitude over wavelength ratio does not change significantly (width 4mm and 0.8mm).

159 Schmittbuhl et al. (2004) could show with their analytical solution that these two roughness  
 160 exponents correspond to two different thermodynamic regimes where surface energy is  
 161 dominant on the small scale and elastic energy dominant on the large scale, with a well-  
 162 defined cross-over length at the millimetre scale.

163 It is important to notice that surface and elastic energies tend to flatten the interface whereas  
 164 the heterogeneities initially present in the host rock i.e. a quenched noise roughen the  
 165 interface (Koehn et al. 2007, Schmittbuhl et al. 2004). The surface energy in the rock stays  
 166 constant whereas the elastic energy is a function of the stress field surrounding the stylolite.  
 167 When the stress increases because the stylolite grows for example in deeper parts of a  
 168 sedimentary basin the elastic energy also increases and the cross-over between surface and  
 169 elastic energy dominated regimes shifts to smaller scales. Hence the influence of surface  
 170 energies is shifted to smaller scales with increasing stress. Determining the cross-over from  
 171 natural stylolites thus gives a value for the stress on the stylolite interface. The scaling  
 172 relation from Schmittbuhl et al. (2004) relates the cross-over length scale ( $l$ ) with the product  
 173 of the mean ( $\sigma_m$ ) and differential ( $\sigma_{dif}$ ) stress according to

$$174 \quad l = \frac{\gamma E}{\beta \sigma_m \sigma_{dif}}, \quad (1)$$

175 where  $\gamma$  is the surface free energy,  $E$  the Young's modulus and  $\beta$  a function of the Poisson  
 176 ratio ( $\beta = \nu(1-2\nu)/\pi$ ). In a sedimentary basin with a uniaxial vertical stress component (i.e.  
 177 zero horizontal displacements) and the horizontal components being a function of the vertical  
 178 stress component  $\sigma_z$ , equation (1) simplifies to (modified after Ebner et al. 2009b)

$$179 \quad l = \frac{\gamma E}{\kappa \sigma_z^2}, \quad (2)$$

180 where  $\kappa$  is a function of the Poisson ratio ( $\kappa = \frac{\nu(1-2\nu)^2(1+\nu)}{3\pi(1-\nu)^2}$ ). This scaling relation is  
 181 only valid for bedding parallel stylolites (sedimentary stylolites), for which the principal



182 horizontal stresses are equal if one assumes no lateral displacement. For tectonic stylolites  
 183 with 3 different main compressive stresses this solution cannot be applied since in that case  
 184 the differential stresses vary. An approximation for the complex tectonic case is given in  
 185 Ebner et al. (2010a). In the present contribution we want to test the scaling relation for  
 186 sedimentary stylolites with the numerical simulations of Koehn et al. (2007) and illustrate  
 187 how the stylolite morphology varies with increasing depth in a sedimentary basin. This  
 188 comparison between natural data (Ebner et al., 2009b), an analytical model (Schmittbuhl et  
 189 al., 2004) and numerical simulations will allow us to propose that stylolites can be used as  
 190 stress gauges.

191

#### 192 **4. Numerical model**

193 We use the numerical model of Koehn et al. (2003, 2006, 2007), Bons et al. (2008) and  
 194 (Ebner et al. 2009a). It is based on a 2D linear elastic lattice spring model where elements can  
 195 dissolve as a function of surface energy, elastic energy and normal stress at the interface.  
 196 Dissolution takes place at a predefined surface that is initially smooth (Fig. 3). Particles on the  
 197 interface are stressed when they are in contact. We calculate the surface energy at the  
 198 interface and the elastic energy of the particle (Koehn et al., 2007) and use these in addition to  
 199 the difference between the normal stress at the particle surface and the average normal stress  
 200 across all particles at the interface to determine how fast the particle dissolves according to  
 201 (Koehn et al., 2007)

$$202 \quad D_i = k_i V_s \left( 1 - \exp \left( \frac{-\Delta \sigma_n V_s - \Delta \psi}{RT} \right) \right), \quad (3)$$

203 where  $D_i$  is the dissolution rate of particle  $i$ ,  $k_i$  a rate constant,  $V_s$  the molecular volume,  $\Delta \sigma_n$   
 204 the difference in normal stress along the interface,  $\Delta \psi_s$  the difference in Helmholtz free  
 205 energy of the solid (the sum of elastic and surface energies at a particle) between a curved  
 206 stressed interface and a flat unstressed interface,  $R$  the universal gas constant and  $T$  the

207 absolute temperature (in Kelvins). Note that we are using the difference in normal stress  
208 between the average normal stress on all interface particles and the particle's normal stress.  
209 We are not using the stress difference between an unstressed surface and a stressed surface. If  
210 we use the difference between an unstressed and a stressed surface the normal stress term is  
211 too dominant and the crossover does not appear in the simulations. We assume that the  
212 structure is constantly dissolving so that diffusion and precipitation of material are not taken  
213 into account. However, since we use the normal stress difference between the average stress  
214 and the local stress we model a situation where the fluid has a concentration of dissolved  
215 material that is proportional to the average normal stress on the stylolite.

216 Roughening of the surface is induced by randomly oriented slower dissolving particles (5%)  
217 that pin the interface until they themselves dissolve (Fig. 3a). In the case of a bimodal grain  
218 size we include slower dissolving larger grains (or fossils), defined by clusters of particles.  
219 These clusters themselves contain a noise on a smaller scale, so that they contain particles that  
220 dissolve slower than the cluster itself (Fig. 3b). For the presented simulations the numerical  
221 model has two resolutions, the smaller resolution of 184000 particles, a real physical width of  
222 4cm and a particle size of 0.1 mm is used for simulations that have a noise and grain size on  
223 one scale whereas a larger resolution of 736000 particles and a real physical width of 8cm is  
224 used for simulations with a bimodal distribution of noise and grain size. Additional  
225 parameters are a Poisson ratio of 0.33 (determined by the shape of lattice used), a Youngs  
226 modulus of 80 GPa and a surface free energy of  $0.27 \text{ J/m}^2$  relevant for limestone. The molar  
227 volume for calcite is  $0.00004 \text{ m}^3/\text{mol}$ , the temperature is 300K and the dissolution constant  
228 for calcite is  $0.0001 \text{ mol}/(\text{m}^2\text{s})$  (Clark, 1966; Renard et al., 2004; Schmittbuhl et al., 2004;  
229 Koehn et al., 2007). The deformation is uniaxial with fixed side-walls simulating stylolite  
230 formation in a sedimentary basin, the vertical stress is constant for the simulation with a  
231 bimodal noise (50 MPa) and is varied between 29 and 92 MPa (29, 41, 50, 57, 64, 71, 80, 92)  
232 for simulations with a noise that is only on the particle scale.

233

## 234 **5. Results of the simulations**

### 235 *5.1. Comparison of natural and simulated stylolites*

236 We use two different initial setups for the simulations, which are illustrated in figure 3. In the  
237 first setup we use a random distribution of slower dissolving particles in the model, these are  
238 shown as dark particles in figure 3a. In all these simulations 5% of particles dissolve 20%  
239 slower than the rest. This means that they can pin the surface, but they may dissolve  
240 themselves if elastic or surface energies at the tips of spikes become too large or if two slower  
241 dissolving particles meet at the interface (Koehn et al., 2007). In the second set of simulations  
242 we add larger grains (also 5%) that dissolve 20% slower (fig. 3b); they are defined as clusters  
243 of particles. These larger grains are added on top of the initial distribution of slower  
244 dissolving particles. This means that the slower dissolving grains also contain particles that  
245 dissolve slower and the noise is bimodal.

246 The developing geometries are shown in figure 4 where we compare the simulated patterns  
247 with natural examples. Figure 4a shows a stylolite that was simulated when using a bimodal  
248 noise. The larger grains at the interface are shown in grey. The stylolite geometry clearly  
249 reflects the bimodal nature of the noise. The largest grains pin the interface and result in  
250 extreme teeth with very straight edges. The stylolite surface between the large grains shows  
251 much smaller roughness amplitude, that slowly develops into larger wavelengths. This surface  
252 is on average still in the middle of the stylolite and resembles the orientation of the initially  
253 flat interface where dissolution started. The teeth that are pinned by larger grains have  
254 variable height depending on when the pinning grains (clusters of slower dissolving particles  
255 in our model setup) meet the interface. The surface on top or at the bottom of the teeth shows  
256 a roughness that is similar to the normal stylolite roughness indicating that the pinning grains  
257 slowly dissolve themselves. The actual dissolution of the host-rock is indicated by the grey  
258 bar on the right hand side of the simulated stylolite. One can observe that the distance

259 between the highest and lowest teeth on each side of the stylolite almost reflects the actual  
260 dissolution. Large grains started to pin the interface relatively early and are not yet completely  
261 dissolved so that the actual dissolution is still recorded by the stylolite. The picture on the  
262 right hand side shows a stylolite from the “Muschelkalk” limestone of southern Germany  
263 where large fossils pin the interface resulting in large teeth. The noise is clearly bimodal and  
264 the simulation captures the geometries of the real stylolite.

265 Figure 4b shows a simulation with a noise only on the particles and a similar natural stylolite  
266 on the right hand side. The simulated stylolite shows the typical geometry that was discussed  
267 in Koehn et al. (2007) and Ebner et al. (2009) with the development of variable wavelengths  
268 and amplitudes of roughness. Extreme spikes can develop if single particles pin the interface  
269 for a long time, meaning that they probably meet no slowly dissolving particle on the other  
270 side of the interface. The spikes are not as straight as the teeth that develop when the noise is  
271 bimodal (Fig. 4a). The grey bar on the right hand side of the simulated stylolite shows the  
272 actual dissolution and illustrate that dissolution is underestimated when the distance between  
273 the highest and lowest tip of the spikes on the stylolite are used to estimate compaction. The  
274 picture on the right hand side of figure 4b shows a stylolite with a geometry that is very  
275 similar to the simulation. This indicates that the noise in the natural example has a relatively  
276 constant scale and the grain size is probably relatively uniform which is underpinned by  
277 microscopic analysis not shown in this study. In general it can be stated that the numerical  
278 model can capture the complex geometries of natural stylolite examples. This implies that the  
279 model captures the main characteristics of stylolite growth and is realistic.

280

## 281 *5.2. Bimodal noise, stylolite growth and compaction estimates*

282 Figure 5 shows the progressive growth of a stylolite with pronounced teeth for three different  
283 time steps, after 2000, 4000 and 6000 model steps. These steps do not correspond to real time  
284 but are a function of the vertical strain and thus the compaction applied to the stylolite – these

285 corresponds to an average of  $xx$ ,  $yy$  and  $zz$  dissolved particle rows. Large grains that pin the  
286 surface are shown in grey and the actual amount of host-rock dissolution is shown in grey  
287 bars on the right hand side of the three stylolites. Grains that pin the interface are initially  
288 relatively close to the starting dissolution surface so that pinning results already in  
289 pronounced teeth in the first time step shown ( $t=2000$ ). Parts of these pinning grains survive  
290 and pin the surface until the last time step. This means that only initially a small part of the  
291 compaction is not recorded by the stylolite but at later stages the teeth record the full amount  
292 of dissolved host-rock. This will change once the pinning grains are dissolved themselves and  
293 pinning stops. During time steps 2000 and 4000 the stylolite geometry is still controlled by  
294 the large pinning grains on the one hand and by the small scale roughness that develops due to  
295 pinning on the particle scale. The latter results in the rough stylolite surface in the centre of  
296 the stylolite at time step 4000 where a number of wavelengths develop. At time step 6000 the  
297 geometry is mainly controlled by the large scale pinning grains since most of these meet with  
298 the stylolite interface. Each tip of a tooth contains small rests of these slower dissolving  
299 grains. Some of the teeth record almost the full compaction (from one side) because they met  
300 the stylolite relatively early and started to grow from the centre of the stylolite. Others,  
301 however, do not really record the full compaction since they either met the interface during a  
302 later stage of growth or they met an already developing tooth and are now dissolving the host-  
303 rock in the other direction. This can be seen for example at time step 2000, when a small grain  
304 on the left hand side of the stylolite meets the left corner of a tooth (see arrow in Fig. 5a). The  
305 grain is now “pushing” upwards into the host-rock, the developing tooth meets the original  
306 orientation of the interface during time step 4000 and moves upwards at time step 6000. One  
307 can use the distance between the highest and lowest tooth in such a stylolite to estimate  
308 compaction. Note that unless two slower dissolving grains are positioned next to each other  
309 but on opposite sides of the stylolite and pin the interface, each stylolite tooth will only record  
310 half of the compaction since they start out from one side of the stylolite (Fig. 5). In contrast to

311 the non-linear growth of stylolites that grow in more uniform rocks (Koehn et al., 2007; Ebner  
312 et al. 2009a), a stylolite with a bimodal noise and strongly pinning grains grows linear with a  
313 growth exponent of about 1.0. – up to the moment where slowly dissolving grains would meet  
314 and destroy this large teeth growing in a ballistic (or fast) mode, to get more fluctuating peak  
315 growth: a transition to a nonlinear growth similar to the more uniform rock type is then  
316 expected.

317

### 318 *5.3. Stress scaling*

319 In the last set of simulations, we perform runs with a uniform noise and vary the stress on the  
320 stylolite. We model stylolites that grew under a vertical stresses of 29, 41, 50, 57, 64, 71, 80  
321 and 92 MPa. All stylolite simulations run for 8000 model time steps, each stress state is  
322 modelled three times. We then analyze the roughness and try to recover the stress from the  
323 stylolite morphology using the crossover length, where we average the results of the three  
324 different runs per stress state. Examples of the finite stylolite pattern are shown in Figure 6,  
325 where we present two stylolites for each stress state from 29 to 80 MPa. Variations in noise in  
326 these cases are only a function of a different random seed of quenched noise i.e. the  
327 heterogeneities in the system for each simulation.

328 Figure 6 illustrates the difficulty to see a relationship between the amount of stress that a  
329 stylolite experienced and the stylolite roughness directly from the geometry of the roughness.  
330 This is also illustrated by the variation in stylolite shape at constant stress depending only on  
331 the random distribution of slowly dissolving particles (right versus left hand side in figure 6).  
332 There may be a general trend from more wavy stylolites at lower stresses to more spiky  
333 stylolites at higher stresses, but this relation is not clear. Therefore one has to use statistical  
334 tools in order to analyze the stylolite roughness.

335 In order to determine the scaling of the interface roughness and cross-over length scale from  
336 the simulated and natural stylolites we use the Fourier method (e.g. Barabasi & Stanley, 1995;

337 Schmittbuhl et al., 1995). We calculate the Fourier power spectrum  $P(k)$  i.e., the square of the  
 338 modulus of the Fourier transform, as a function of the wave-number  $k$  [1/lengthscale ( $\text{mm}^{-1}$ )]  
 339 for each stylolite pattern. For the simulations we take averages of the power spectra of three  
 340 runs and plot the resulting average power spectrum as a function of  $k$  in log-log space. If the  
 341 roughness is self-affine the plot shows (Fig. 3) a linear slope, which is a function of the Hurst  
 342 exponent (Renard et al., 2004; Schmittbuhl et al., 2004)

$$343 \quad P(k) \sim k^{-1-2\alpha}. \quad (4)$$

344 Figure 7a shows the power spectrum as a function of the wave-number for the natural stylolite  
 345 of figure 1 and figure 7b an average of three numerical simulations. Both plots are similar,  
 346 with the natural data spanning over a wider range of magnitudes than the simulated data but  
 347 the simulated data having less noise in the signal because it is averaged over three runs. Since  
 348 the wave-number in the plots is a function of 1/wavelength, the left hand side of the plots  
 349 represents the larger wavelengths. Here the plots show two slopes, separated by a well-  
 350 defined crossover wavelength. These two self-affine regimes correspond to the elastic energy  
 351 dominated regime at the large scale and the surface energy dominated regime at the small  
 352 scale. On the very right hand side of the two plots the slope becomes flatter at a length scale  
 353 comparable to the particle size in the model and the drawn bitmap of the natural example.  
 354 This flat portion of the signal has to be cut off for the analysis of the cross-over length scale.  
 355 In order to fit a curve to the graphs we bin the data: it becomes clear in Figure 7c and d that in  
 356 the binned data set the two slopes become more visible. To avoid bias due to improper fitting  
 357 of the crossover-length that separates the two slopes we use a nonlinear least square curve-  
 358 fitting algorithm in logarithmic space (Ebner et al. 2009b) with predefined roughness  
 359 exponents of 1.1 and 0.5 for the surface energy and elastic dominated regimes, respectively  
 360 (Ebner et al., 2009b). The resulting cross-over  $l$  is then used for further analysis.

361 Figure 8 shows the result of the 24 simulations where the vertical stress component of the  
 362 simulated stylolites is plotted against the inverse of the square root of the cross-over

363 according to the scaling function of equation (2). The determined cross-over in the  
364 simulations is clearly a function of the stress on the stylolite and shows the right scaling  
365 relation:

$$366 \quad \sigma_z = a\sqrt{1/l}, \quad (5)$$

367 similarly to equation (2), since the boundary condition used in these simulations also  
368 correspond to a fixed vertical stress and fixed lateral displacement along x, as the one used to  
369 derive equation (2). The slope ( $a$ ) of the linear regression line of the data is a function of the  
370 input parameters in equation (2) of the numerical model. The slope is almost identical with  
371 the input parameters of the numerical model (square root of Young's modulus times surface  
372 energy divided by  $\kappa$ ), which shows that the scaling relation derived analytically and presented  
373 by Schmittbuhl et al. (2004) is verified by the numerical stylolite morphologies and is  
374 independently produced by the current numerical model presented here. This thus constitutes  
375 another completely independent check of this analytical expression, after the comparison of  
376 the overload stresses with the one determined from the crossover length for the stylolites  
377 investigated by Ebner et al. (2009b) in Southern France.

378

## 379 **6. Methodology and application to natural cases**

380 As an example for a paleo-stress calculation, we can use the natural stylolite shown in Figure  
381 1 and the determined cross-over in Figure 7c. The calculation gives a vertical stress of about  
382 34 MPa, a horizontal stress of about 13 MPa, a mean stress of 23.5 MPa and a differential  
383 stress of 21 MPa. If we assume that the overlying sediments in the basin had a density of  
384 about 2.5 kg/cm<sup>3</sup>, the paleo-depth of the stylolite was about 1400 m in the basin. The  
385 orientation of the teeth or spikes of the stylolite indicates that the direction of the main  
386 compressive stress was vertical and that the stylolite formed in the sedimentary basin during  
387 burial. A limit with these calculations will always be the uncertainty in the input parameters



388 like the Young's Modulus, Poisson's ratio and the surface free energy at the time of stylolite  
 389 formation. We used a relatively high Young's Modulus for the numerical simulations (80  
 390 GPa). The real limestone may have a lower value of about 50 GPa and this would change the  
 391 stress and depth estimates (26.5 MPa vertical stress and 1100 m overburden). It is always  
 392 advisable to use a range of natural stylolites for depth estimates as proposed in the work of  
 393 Ebner et al. (2009b). In addition to the stress calculation, one can estimate the amount of  
 394 dissolved material at the stylolite. According to the presented simulations the stylolite shown  
 395 in figures 1 and 4b (right hand side) developed in a host-rock with a relatively uniform grain  
 396 size. If the stylolite grew in a similar way than the simulations (Fig. 4b) then the dissolved  
 397 material at the interface is in the order of 3 cm. However, since the grain size in the natural  
 398 example is about 1/10<sup>th</sup> of the size of the model particles, the actual amount of dissolved  
 399 material at the interface is probably larger, because the amount of dissolved material depends  
 400 on the grain size (equation 6). The scaling relation of Koehn et al. (2007)

$$401 \quad A = b \left( \frac{w}{L} \right)^{1/0.8} L, \quad (6)$$

402 where the prefactor  $b$  is 10 (factor varies, see Koehn et al., 2007 and Ebner et al., 2009a),  $A$  is  
 403 the dissolved material (mm),  $w$  the mean RMS width of the interface in millimeter (for details  
 404 of calculation compare Koehn et al., 2007 and Ebner et al., 2009a) and  $L$  the grain size (mm),  
 405 with a grain size of about 0.01 mm for the natural example and a mean width of the interface  
 406 of 2mm, results in an estimation of roughly 7.5 cm of material dissolved at the interface or 40  
 407 times the mean width of the interface. It is thus not possible to deduce the amount of  
 408 dissolution directly from the finite interface morphology.

409

## 410 **7. Conclusions**

411 We modelled the development of stylolite patterns using a rock matrix that contains either a  
 412 uniform or a bimodal grain size. Stylolites that developed from a bimodal noise show

413 pronounced teeth with straight edges and grow linearly with a growth exponent of about 1.0.  
414 The morphology produced by the simulations is similar to field observations. The distance  
415 between the maximum and minimum height of a tooth above and below the original  
416 dissolution surface can be used to estimate compaction if pinning starts relatively early during  
417 stylolite growth, and pinning grains are not completely destroyed during successive  
418 dissolution, thus giving a value that only slightly underestimates the true dissolution along the  
419 interface. Stylolites that develop in a rock that has a noise that sits on a uniform grain size  
420 may contain spikes but the height of these asperities highly underestimates compaction. For  
421 these stylolites the mean width of the interface should be calculated and the scaling law of  
422 Koehn et al. (2007) should be used to estimate compaction.

423 Modelling the growth of stylolites that developed under different normal stresses shows  
424 stylolite patterns that can be best distinguished using statistical methods. We use the Fourier  
425 method to extract the cross-over length scale from the numerical stylolites, calculate the  
426 predicted theoretical vertical stress values and compare them with the actual values used in  
427 the numerical simulations. The results are consistent and we can show that the numerical  
428 model reproduces the proposed scaling relation, thus our numerical model gives an  
429 independent confirmation of the analytical solution of Schmittbuhl et al. (2004). This  
430 analytical solution to determine paleo-stress magnitudes from stylolite shapes seems to be  
431 robust: the analytical result is verified for sets of stylolites obtained with two independent  
432 techniques, namely the ones produced with the current numerical model, and natural  
433 examples investigated by Ebner et al. (2009), whose burial stresses were inferred from their  
434 relative position in the stratigraphic column. To summarize, comparing numerical simulations  
435 with the stylolite shown on Figure 1b indicates that this stylolite formed during burial in a  
436 basin, at depth close to 1400 m, and accommodated about 7.5 cm of dissolution.

437

438 Acknowledgements

439 Koehn and Ebner acknowledge funding by the DFG (KO 2114/5). Toussaint and Renard  
440 acknowledge support of a FORPRO CNRS/ANDRA grant.

441

## 442 References

- 443 Aharonov, E., Katsman, R., 2009. Interaction between pressure solution and clays in stylolite  
444 development: insights from modeling. *American Journal of Science* 309, 7, 607-632.
- 445 Barabasi, A. L., Stanley, H. E., 1995. *Fractal concepts in surface growth*. Cambridge  
446 University Press.
- 447 Baron M., Parnell J., 1979. Relationships between stylolites and cementation in sandstone  
448 reservoirs: Examples from the North Sea, UK and East Greenland. *Sedimentary*  
449 *Geology* 194, 17-35.
- 450 Beach, A., 1979. Pressure solution as a metamorphic process in deformed terrigenous  
451 sedimentary rocks. *Lithos* 12, 51-58.
- 452 Bons, P. D., Koehn, D., Jessell, M. W., 2008. *Microdynamics Simulation*. In: *Lecture Notes*  
453 *in Earth Sciences* 106. Springer, Berlin.
- 454 Brouste, A., Renard, F., Gratier, J. P., Schmittbuhl, J., 2007. Variety of stylolites'  
455 morphologies and statistical characterization of the amount of heterogeneities in the  
456 rock. *Journal of Structural Geology* 29, 422-434.
- 457 Burkhard M., 1993. Calcite twins, their geometry, appearance and significance as stress-strain  
458 markers and indicators of tectonic regime: a review. *J. Struct. Geol.* 15, 3-5, 351-368.
- 459 Clark, S. P. J., 1966. *Handbook of Physical Constants*. Geological Society of America, New  
460 York.
- 461 Dunnington, H. V., 1954. Stylolite development post-dates rock induration. *Journal of*  
462 *sedimentary Petrology* 24, 27-49.
- 463 Ebner, M., Koehn, D., Toussaint, R., Renard, F., 2009a. The influence of rock heterogeneity  
464 on the scaling properties of simulated and natural stylolites. *Journal of Structural*  
465 *Geology* 31, 72-82.
- 466 Ebner, M., Koehn, D., Toussaint, R., Renard, F., Schmittbuhl, J., 2009b. Stress sensitivity of  
467 stylolite morphology. *Earth and Planetary Science Letters* 277, 394-398.
- 468 Ebner, M., Toussaint, R., Schmittbuhl, J., Koehn, D., Bons, P. 2010a. Anisotropic scaling of  
469 tectonic stylolites: a fossilized signature of the stress field? *J. Geophys. Res.* 115,  
470 B06403.
- 471 Ebner, M., Piazzolo, S., Renard, F., Koehn, D., 2010b. Stylolite interfaces and surrounding  
472 matrix material: Nature and role of heterogeneities in roughness and microstructural  
473 development. *Journal of Structural Geology* 32, 1070-1084.
- 474 Fabricius, I.L., Borre, M.K., 2007. Stylolites, porosity, depositional texture and silicates in  
475 chalk facies sediments. *Ontong Java Plateau – Gorm and Tyra fields, North Sea.*  
476 *Sedimentology* 54, 183-205.
- 477 Fletcher, R. C., Pollard, D. D., 1981. Anti-Crack Model for Pressure Solution Surfaces.  
478 *Geology* 9, 419-424.
- 479 Gratier, J. P., Muquet, L., Hassani, R., Renard, F., 2005. Experimental microstylolites in  
480 quartz and modeled application to natural stylolitic structures. *Journal of Structural*  
481 *Geology* 27, 89-100.
- 482 Guzzetta, G., 1984. Kinematics of Stylolite Formation and Physics of the Pressure-Solution  
483 Process. *Tectonophysics* 101, 383-394.
- 484 Heald, M. T., 1955. Stylolites in Sandstones. *Journal of Geology* 63, 101-114.

485 Katsman, R., Aharonov, E., Scher, H., 2006. A numerical study on localized volume  
486 reduction in elastic media: some insights on the mechanics of anticracks, *JGR*, 111,  
487 B3, B03204.

488 Karcz, Z., Scholz, C. H., 2003. The fractal geometry of some stylolites from the Calcare  
489 Massiccio Formation, Italy. *Journal of Structural Geology* 25, 1301-1316.

490 Koehn, D., Arnold, J., Jamtveit, B., Malthe-Sørenssen, A., 2003. Instabilities in stress  
491 corrosion and the transition to brittle failure. *American Journal of Science* 303, 956-  
492 971.

493 Koehn, D., Malthe-Sørenssen, A., Passchier, C.W., 2006. The structure of reactive grain  
494 boundaries under stress containing confined fluids. *Journal of Chemical Geology* 230,  
495 207-219.

496 Koehn, D., Renard, F., Toussaint, R., Passchier, C. W., 2007. Growth of stylolite teeth  
497 patterns depending on normal stress and finite compaction. *Earth and Planetary  
498 Science Letters* 257, 582-595.

499 Lacombe, O., 2010. Calcite Twins, a Tool for Tectonic Studies in Thrust Belts and Stable  
500 Orogenic Forelands, *Oil & Gas Science and Technology – Rev. IFP Energies  
501 nouvelles*, 65, 809-838.

502 Merino, E., 1992. Self-organization in stylolites. *American Scientist* 80, 466.

503 Park, W. C., Schot, E. H., 1968. Stylolites: their nature and origin. *Journal of sedimentary  
504 Petrology* 38, 175-191.

505 Petit, J. P., Mattauer, M., 1995. Paleostress Superimposition Deduced from Mesoscale  
506 Structures in Limestone - the Matelles Exposure, Languedoc, France. *Journal of  
507 Structural Geology* 17, 245-256.

508 Railsback, L. B., 1993. Lithologic Controls on Morphology of Pressure-Dissolution Surfaces  
509 (Stylolites and Dissolution Seams) in Paleozoic Carbonate Rocks from the Mideastern  
510 United-States. *Journal of Sedimentary Petrology* 63, 513-522.

511 Renard, F., Schmittbuhl, J., Gratier, J. P., Meakin, P., Merino, E., 2004. Three-dimensional  
512 roughness of stylolites in limestones. *Journal of Geophysical Research-Solid Earth*  
513 109 (B3).

514 Rispoli, R., 1981. Stress-Fields About Strike-Slip Faults Inferred from Stylolites and Tension  
515 Gashes. *Tectonophysics* 75, T29-T36.

516 Rutter, E. H., 1983. Pressure solution in nature, theory and experiment. *Journal of the  
517 Geological Society of London* 140, 725-740.

518 Schmittbuhl, J., Vilotte, J. P., Roux, S., 1995. Reliability of Self-Affine Measurements.  
519 *Physical Review E* 51, 131-147.

520 Schmittbuhl, J., Renard, F., Gratier, J. P., Toussaint, R., 2004. Roughness of stylolites:  
521 Implications of 3D high resolution topography measurements. *Physical Review  
522 Letters* 93, 238501.

523 Tada, R., Siever, R., 1989. Pressure Solution during Diagenesis. *Annual Review of Earth and  
524 Planetary Sciences* 17, 89-118.

525

526 Figure captions

527 Figure 1: Example of the same natural stylolite in limestone, at different scales. On the large  
528 scale, the stylolite is relatively flat whereas the aspect ratio of the roughness (out-of-plane  
529 dimension over in-plane one) increases towards smaller scales from a to c. Between c and d  
530 the roughness aspect ratio remains constant.

531

532 Figure 2: a) Sketch showing typical stylolite teeth where the sides of the teeth are oriented  
533 parallel to the main compressive stress. In the example on the right hand side the teeth are  
534 inclined indicating that the main stylolite plane is oriented at an angle to the smallest principle  
535 stress  $\sigma_3$ . b) Sketch illustrating how stylolite teeth shown in a) can grow if impurities (dark  
536 circles) pin the interface. c) Sketch after Ebner et al. (2010b) showing how low solubility  
537 quartz grains may pin the sides of teeth in natural stylolites.

538

539 Figure 3: Model setups for the numerical simulations of stylolite roughening. The sidewalls  
540 are confined and the upper and lower walls are pushed inwards. Dissolution takes place along  
541 an initially flat line in the centre of the model. Dark particles dissolve slower. a) Setup for a  
542 uniform grain size where the particles in the model may represent grains in the rock. b) Setup  
543 for a bimodal grain size, where the small grains are represented by particles in the model  
544 whereas the large grains are defined by clusters of particles.

545

546 Figure 4: Results of the numerical simulations of stylolite roughening for a) a bimodal grain  
547 size and b) a uniform grain size. The actual dissolution of the host rock is indicated with grey  
548 vertical bars next to the stylolites. On the right hand side two natural stylolites are shown that  
549 may represent similar variations in noise than in the simulations. The grey patches along the  
550 stylolite indicate the largest grains that dissolve slower and act as pinning sites for the  
551 interface. Note the strong similarity between the numerical simulations and the natural  
552 stylolites.

553

554 Figure 5: Time sequence of simulated stylolite growth in a host rock with a bimodal grain  
555 size. Note that model steps are proportional to strain increments and amounts of dissolved  
556 material and not real time. Bars on the right hand side record the real amount of dissolved

557 material in the simulations. Note how largest grains (grey patches) pin the interface and  
558 produce pronounced teeth that record accurately the actual compaction.

559

560 Figure 6: Two sets of 7 stylolites that developed under increasing normal stress. Right and left  
561 hand stylolites only differ in initial random seeds of the quenched noise in the simulations.

562 The relationship between the rough geometries and stresses cannot be visualized, even though  
563 there may be an increase in spikes from low to high stresses.

564

565 Figure 7: Fourier analysis of the roughness of stylolites, where the Fourier power spectrum  
566 ( $P(k)$ ) is plotted against the wave-number ( $k$ ), the inverse of the wavelength of the roughness.

567 a) shows a Fourier analysis of a the natural stylolite shown in figure 1, b) an average of the

568 Fourier analysis of 3 numerical stylolites. c) and d) show binned data sets of the Fourier

569 power spectra of a) and b) and the presence of a well-defined crossover length scale.

570

571 Figure 8: Plot of the square root of the inverse of the determined crossover length from the

572 numerical simulations against the applied stress following the scaling law of Schmittbuhl et

573 al., (2004). The data plots roughly on a line illustrating that the simulations reproduce the

574 scaling relation. Error bars represent variations in different cross-over length scales found in

575 different simulations.

## \*Highlights

Stylolites are stress gauges

Stylolites can be used to estimate compaction

Grain size distribution influences stylolite teeth growth

Stylolites with large pinning fossils grow linear

Stylolites with uniform grain size grow non-linear

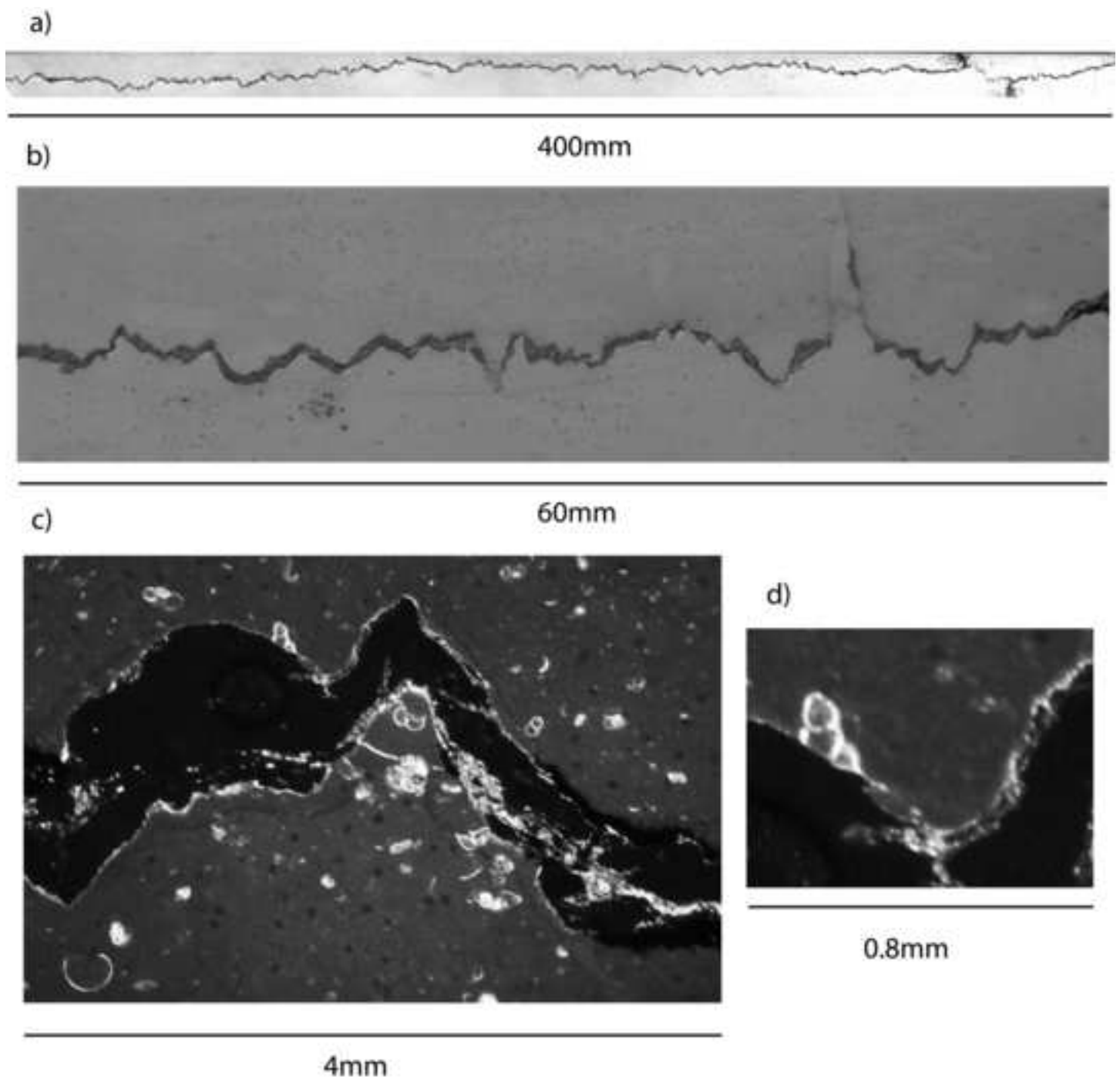


Fig. 1



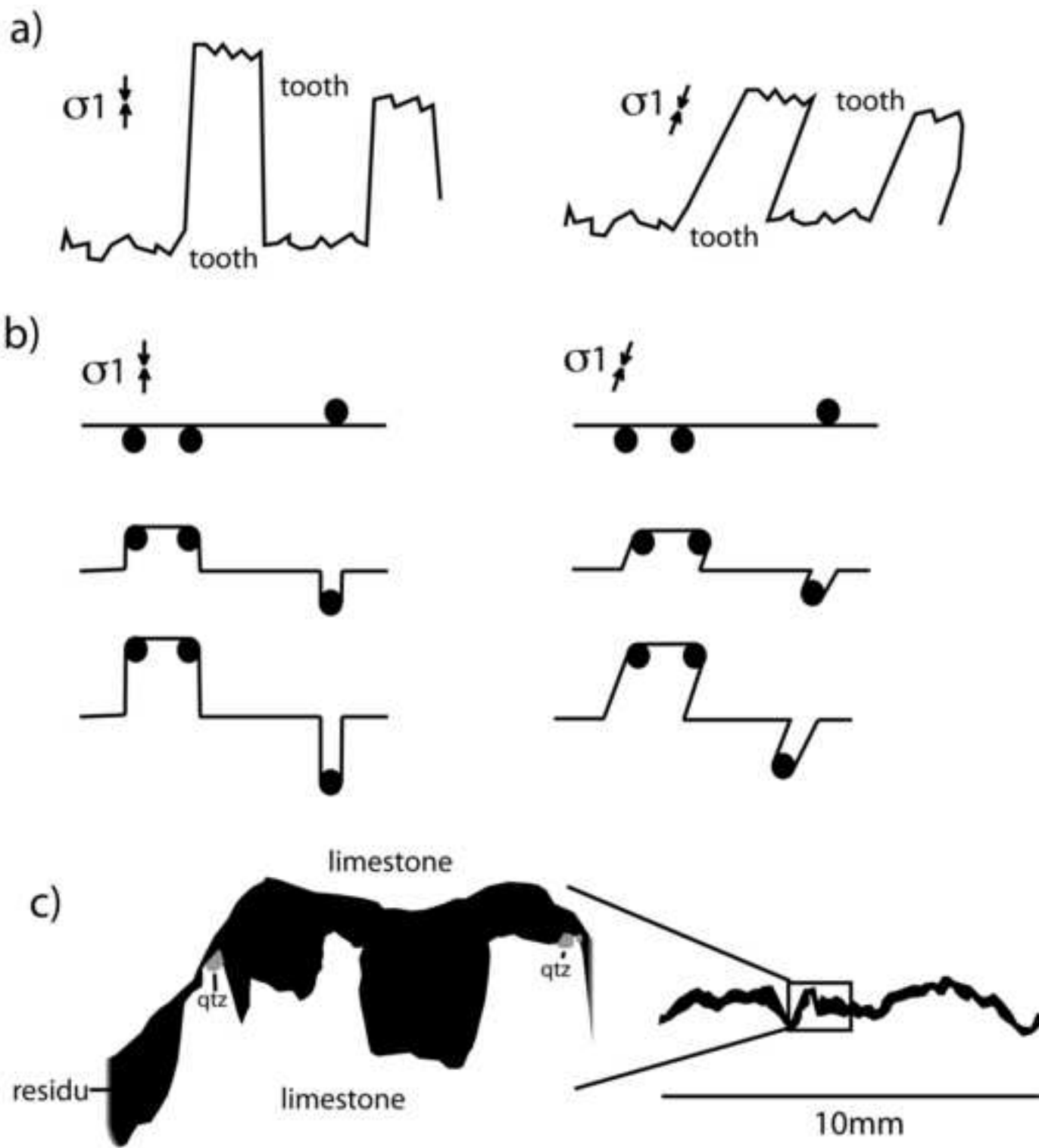


figure 2

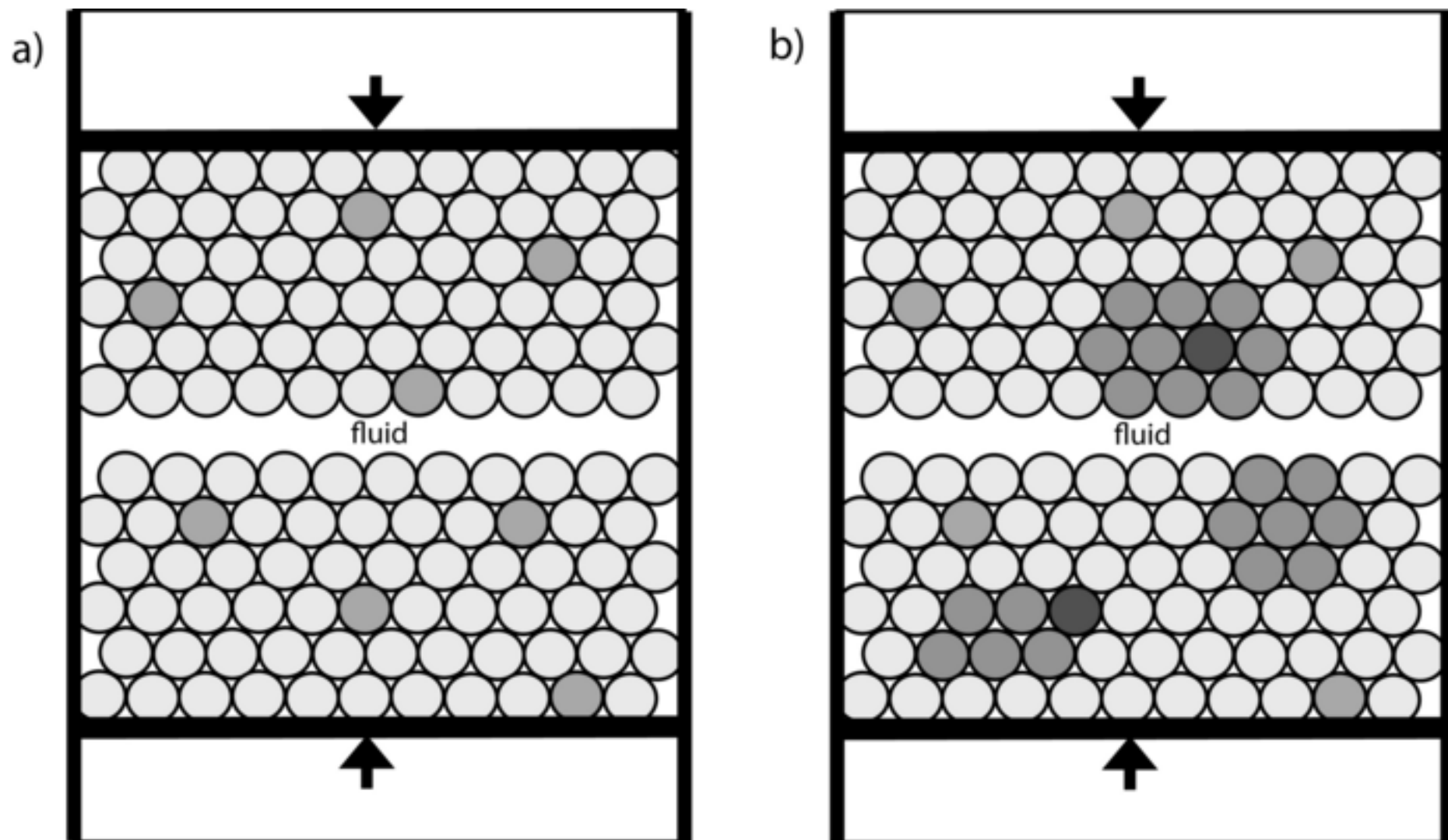


Figure 3

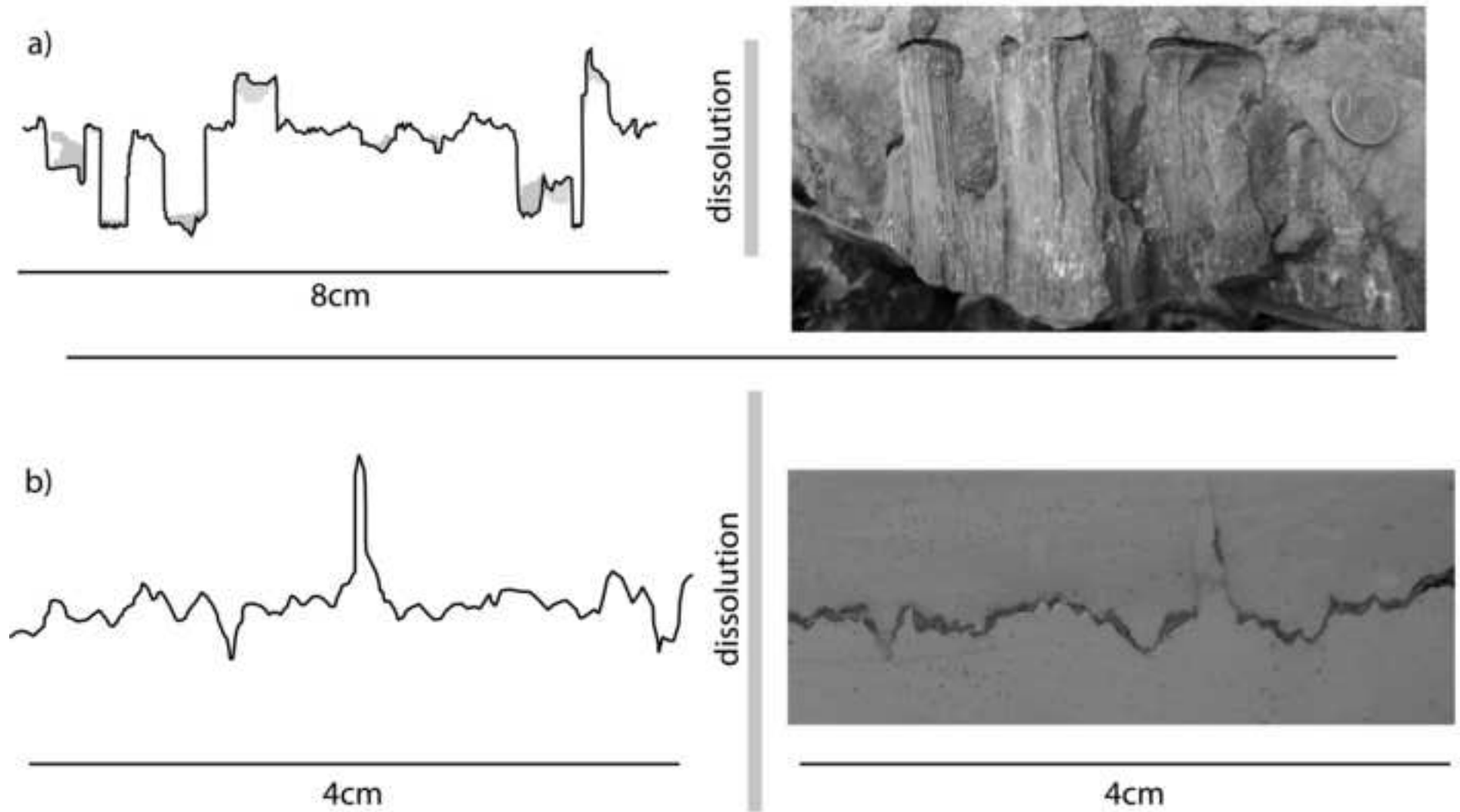


figure 4

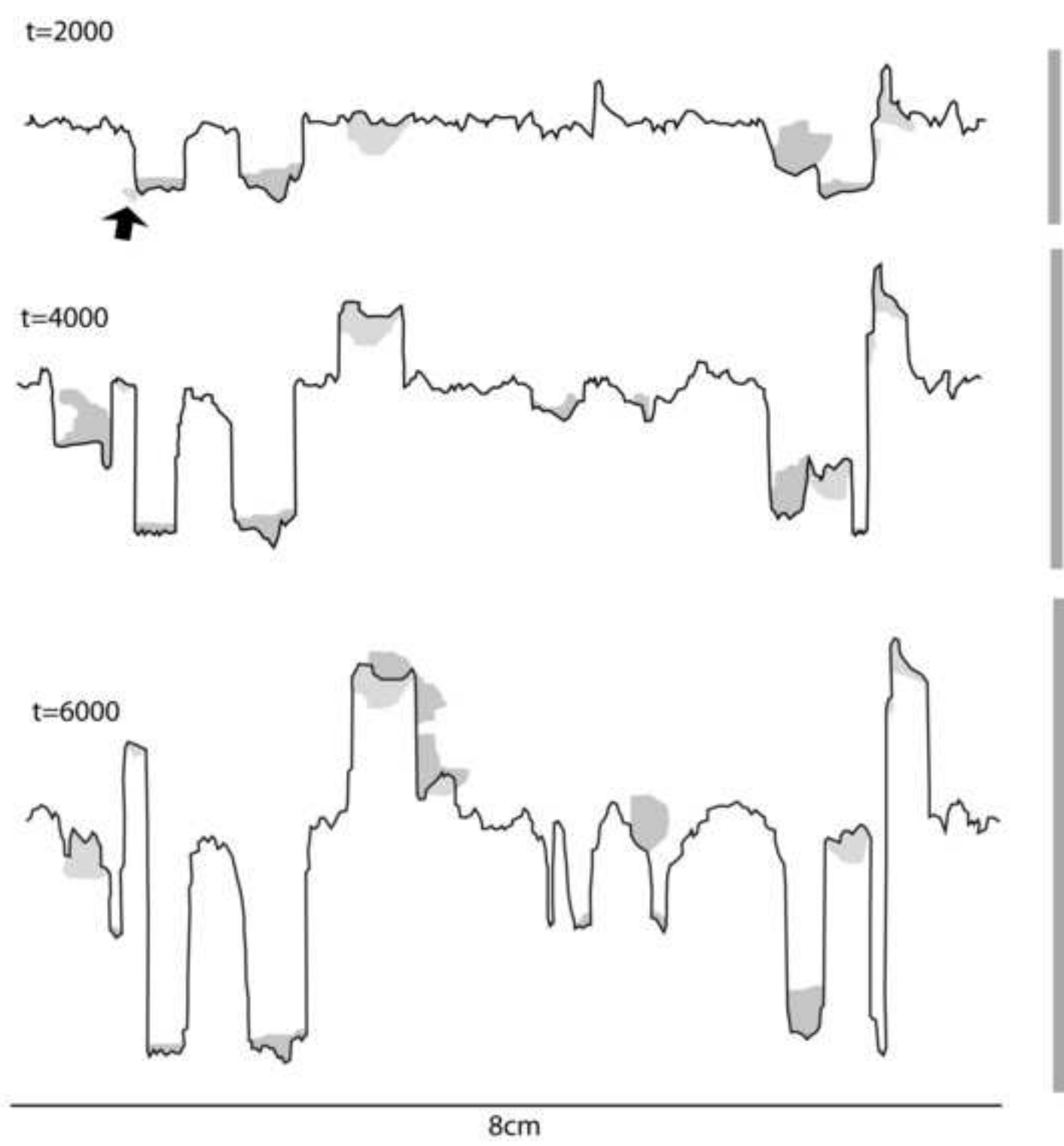


figure 5

Figure

[Click here to download high resolution image](#)

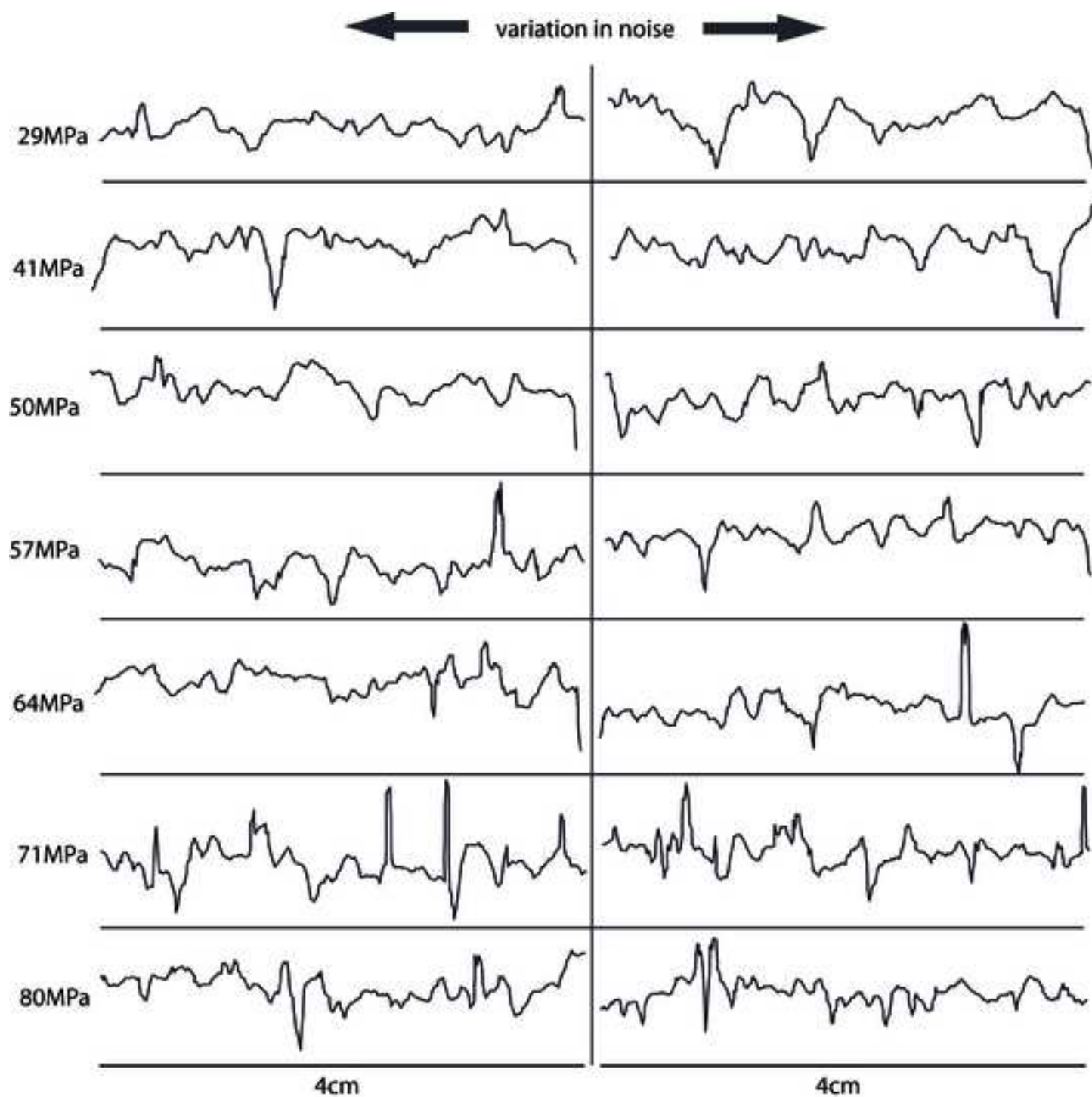


figure 6

Figure

[Click here to download high resolution image](#)

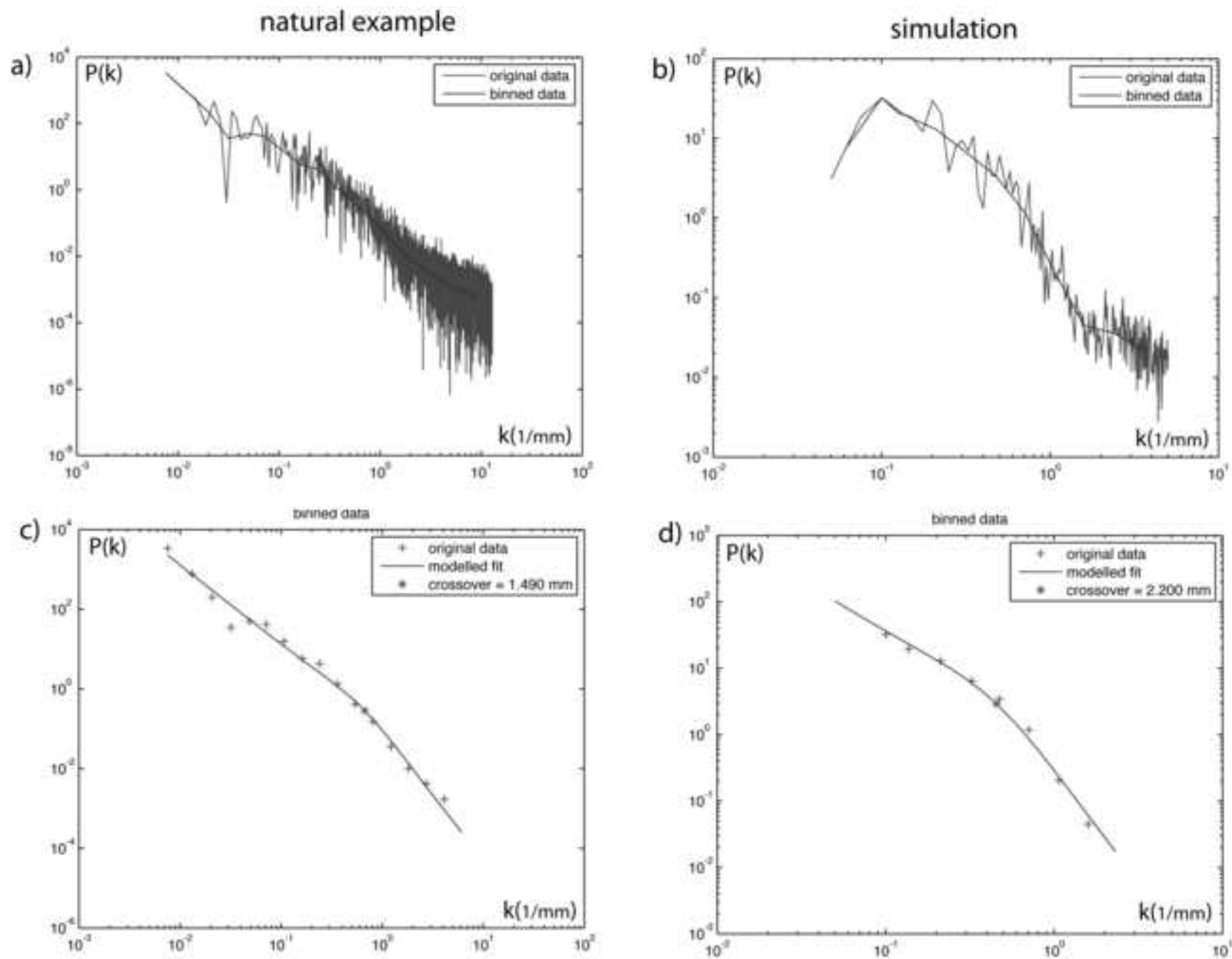


figure 7

Figure  
[Click here to download high resolution image](#)

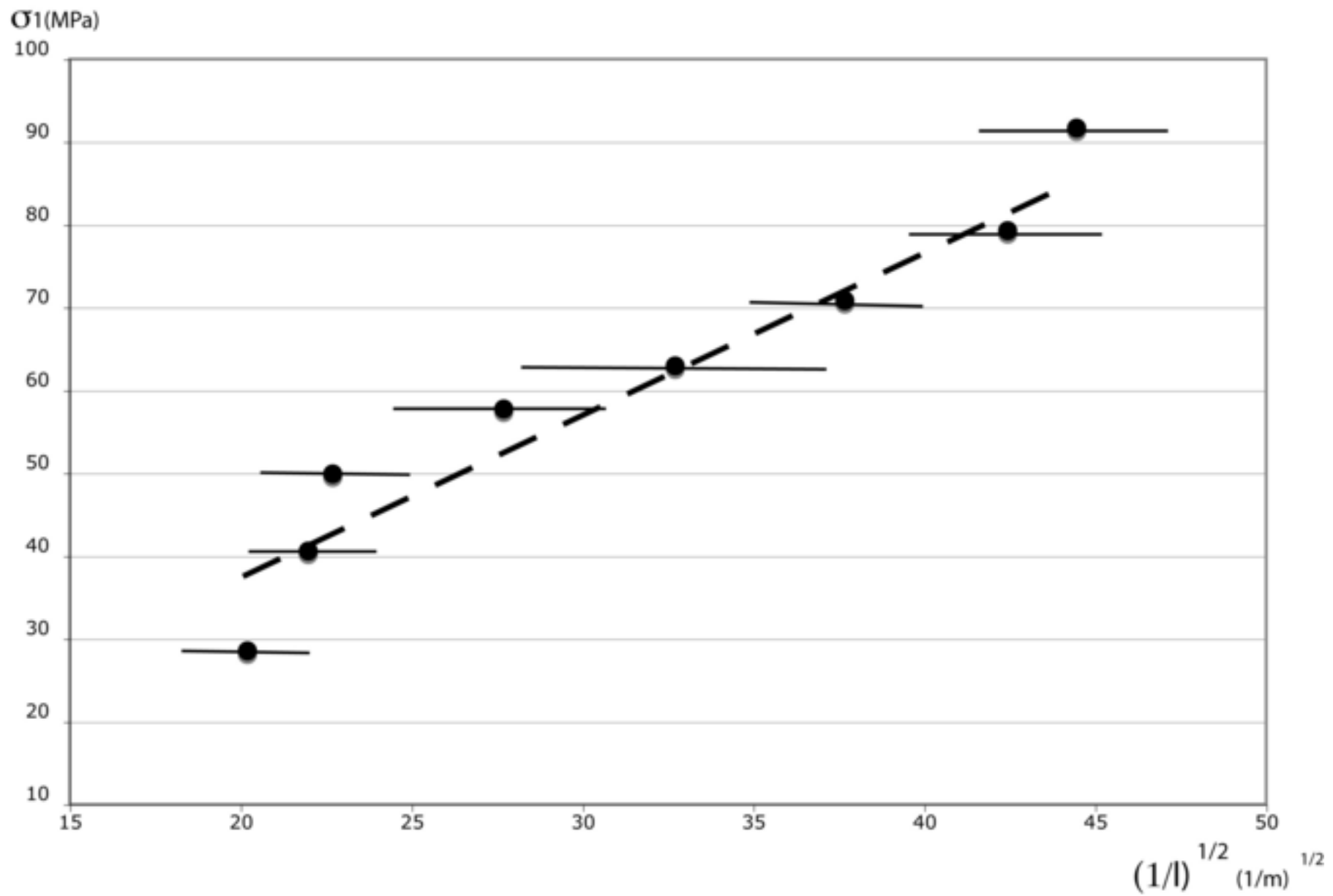


figure 8